Journal of Receptors and Signal Transduction

ISSN: (Print) (Online) Journal homepage: https://www.tandfonline.com/loi/irst20

Discovery of polymethoxyflavones as potential cyclooxygenase-2 (COX-2), 5-lipoxygenase (5-LOX) and phosphodiesterase 4B (PDE4B) inhibitors

Muhd Hanis Md Idris, Siti Norhidayah Mohd Amin, Siti Norhidayu Mohd Amin, Agustono Wibowo, Zainul Amiruddin Zakaria, Zurina Shaameri, Ahmad Sazali Hamzah, Manikandan Selvaraj, Lay Kek Teh & Mohd Zaki Salleh

To cite this article: Muhd Hanis Md Idris, Siti Norhidayah Mohd Amin, Siti Norhidayu Mohd Amin, Agustono Wibowo, Zainul Amiruddin Zakaria, Zurina Shaameri, Ahmad Sazali Hamzah, Manikandan Selvaraj, Lay Kek Teh & Mohd Zaki Salleh (2021): Discovery of polymethoxyflavones as potential cyclooxygenase-2 (COX-2), 5-lipoxygenase (5-LOX) and phosphodiesterase 4B (PDE4B) inhibitors, Journal of Receptors and Signal Transduction, DOI: 10.1080/10799893.2021.1951756

To link to this article: https://doi.org/10.1080/10799893.2021.1951756

JOURNAL OF RECEPTORS AND SIGNAL TRANSDUCTION
https://doi.org/10.1080/10799893.2021.1951756

Taylor & Francis
Taylor & Francis Group

RESEARCH ARTICLE

Discovery of polymethoxyflavones as potential cyclooxygenase-2 (COX-2), 5-lipoxygenase (5-LOX) and phosphodiesterase 4B (PDE4B) inhibitors

Muhd Hanis Md Idris[a], Siti Norhidayah Mohd Amin[a], Siti Norhidayu Mohd Amin[a], Agustono Wibowo[b], Zainul Amiruddin Zakaria[c], Zurina Shaameri[d], Ahmad Sazali Hamzah[d], Manikandan Selvaraj[e], Lay Kek Teh[a] and Mohd Zaki Salleh[a]

[a]Integrative Pharmacogenomics Institute (iPROMISE), Universiti Teknologi MARA (UiTM) Selangor Branch, Puncak Alam Campus, Selangor, Malaysia;[b]Faculty of Applied Science, Universiti Teknologi MARA (UiTM) Pahang Branch, Jengka Campus, Pahang, Malaysia; [c]Department of Biomedical Science, Faculty of Medicine and Health Sciences, Universiti Putra Malaysia (UPM), Serdang, Malaysia; [d]Organic Synthesis Laboratory, Institute of Science (IOS), Universiti Teknologi MARA (UiTM) Selangor Branch, Puncak Alam Campus, Selangor, Malaysia; [e]School of Engineering, Monash University (Malaysia Campus), Bandar Sunway, Malaysia

ABSTRACT

Non-steroidal anti-inflammatory drugs (NSAIDs) are widely prescribed to treat inflammatory-related diseases, pain and fever. However, the prolong use of traditional NSAIDs leads to undesirable side effects such as gastric, ulceration, and renal toxicity due to lack of selectivity toward respective targets for COX-2, 5-LOX, and PDE4B. Thus, targeting multiple sites can reduce these adverse effects of the drugs and increase its potency. A series of methoxyflavones (**F1**–**F5**) were synthesized and investigated for their anti-inflammatory properties through molecular docking and inhibition assays. Among these flavones, only **F2** exhibited selectivity toward COX-2 (Selectivity Index, SI: 3.90, COX-2 inhibition: 98.96 ± 1.47%) in comparison with celecoxib (SI: 7.54, COX-2 inhibition: 98.20 ± 2.55%). For PDEs, **F3** possessed better selectivity to PDE4B (SI: 4.67) than rolipram (SI: 0.78). **F5** had the best 5-LOX inhibitory activity among the flavones (33.65 ± 4.74%) but less than zileuton (90.81 ± 0.19%). Docking analysis indicated that the position of methoxy group and the substitution of halogen play role in determining the bioactivities of flavones. Interestingly, **F1**–**F5** displayed favorable pharmacokinetic profiles and acceptable range of toxicity (IC_{50}>70 μM) in cell lines with the exception for **F1** (IC_{50}: 16.02 ± 1.165 μM). This study generated valuable insight in designing new anti-inflammatory drug based on flavone scaffold. The newly synthesized flavones can be further developed as future therapeutic agents against inflammation.

GRAPHICAL ABSTRACT

ARTICLE HISTORY
Received 3 January 2021
Revised 27 June 2021
Accepted 30 June 2021

KEYWORDS
Flavonoids synthesis; molecular docking; multi-target inhibitor; inflammatory; pharmacokinetics; cytotoxicity

Introduction

Inflammation is a natural protective body response to harmful stimuli, such as pathogens, damaged cells, or irritants, to eliminate initial cause of injury, clear out necrotic cells and damaged tissue, and initiate tissue repair. However, chronic uncontrolled inflammation is harmful as it damages host tissues and causes inflammatory diseases such as cancers, diabetes, and rheumatoid arthritis [1]. Inflammation is closely associated with pro-inflammatory enzymes including cyclooxygenases (COX), lipoxygenases (LOX), and phosphodiesterases (PDE), in addition to other pro-inflammatory mediators and cytokines including prostaglandin E2, interleukins IL-1, IL-6, and IL-8, and tumor necrosis factor (TNF-α) [2–4]. Therefore, many studies are focusing on these inflammatory markers as drug target to treat inflammatory diseases.

Non-steroidal anti-inflammatory drugs (NSAIDs) and COX-2 inhibitors are the most widely used drug for reducing inflammation and pain. The drugs inhibit COX and stop arachidonic acid from transforming into prostaglandins, thromboxane, and prostacyclin. The traditional nonselective non-steroidal anti-inflammatory drugs such as ibuprofen and naproxen are capable of inhibiting both COX-1 and COX-2 isoforms [5]. Nevertheless, adverse gastrointestinal events such as gastric mucosal damage and gastroduodenal ulcers have been reported due to the use of the non-steroidal anti-inflammatory drugs. More selective COX-2 inhibitors were developed to minimize the side effects but chronic use of some of these inhibitors still cause cardiovascular adverse effects and increase thrombotic risk due to blockage of prostaglandin I_2 [6]. In addition, PDE4 inhibitors that are used for treating inflammation have been discontinued due to side effects such as emesis, mild to moderate nausea, headache, and diarrhea [7]. The only 5-LOX inhibiting drug, known as zileuton, was also withdrawn from the market due to its hepatotoxicity adverse effect [8].

Flavone is among the major plant secondary metabolites that are broadly distributed across the plant kingdom. It

CONTACT Mohd Zaki Salleh zakisalleh@uitm.edu.my Integrative Pharmacogenomics Institute (iPROMISE), Universiti Teknologi MARA (UiTM) Selangor, Puncak Alam Campus, Bandar Puncak Alam 42300, Malaysia

Supplemental data for this article can be accessed here.

consists of a phenyl ring that attaches to chromone at 2-position. With a high degree of chemical diversity by modifications of the chemical backbones, flavone and its derivatives have multiple roles in biological functions and attract great interest from the researchers as privilege structures in drug discovery [9, 10]. In recent years, *in vitro* and *in vivo* studies as well as clinical studies have reported flavones as anti-inflammatory agent [11–13]. For instance, flavones displayed the reduction of COX-2 mediated prostaglandin E2 (PGE2) production and inhibited the activity of 5-lipoxygenase (5-LOX) [14]. Another study also reported that natural flavone was able to inhibit formation of nitric oxide (NO) in lipopolysaccharide (LPS)-activated RAW 264.7 macrophages and indicated as potent anti-lipoxygenase inhibitor without significant cytotoxic effect [15].

The structure–activity analysis showed that the substitution at 5 and 7 positions of ring A and at 4′ position of ring B and the presence of C2–C3 double bond are crucial in determining their anti-inflammatory effects. Additionally, the oxidation of flavones into reactive electrophilic quinones can interact with nucleophilic natured thiols and amino groups of proteins. This leads to the formation of different additional products that are responsible for their valuable biological effects [16, 17]. In our previous study, isolated flavones from *Muntingia calabura* possessed anti-nociceptive and anti-inflammatory activity by regulating inflammatory response through cAMP pathway [18]. The ability of flavones to mimic cAMP stacking interaction in PDE makes flavones good competitive PDE inhibitors which elevates level of cAMP. Besides, the functional group at C-4′ position also plays important role in inhibiting PDE [19]. Therefore, the present study is a continuation of our previous work to further investigate the inhibitory potential of flavones toward multi-targets of COX-2, 5-LOX, and PDE4B as well as pharmacokinetic and toxicity profiles of the synthesized flavones.

Methods

Chemistry

Solvents and chemicals were purchase from Sigma-Aldrich (St. Louis, MO) unless otherwise stated. The ^{1}H and ^{13}C NMR spectra were registered in $CDCl_3$ with Joel Resonance ECZ400S [400 MHz (^{1}H) and 100 MHz (^{13}C)] using TMS as the internal standard. Analytical TLC was performed on silica gel $60F_{254}$, Merck (layer thickness 0.25 mm, Merck, Kenilworth, NJ) and visualized with UV light and $KMnO_4$ as the detecting agent.

Synthesis of iodoacetophenone

About 1.0 M solution of iodine chloride (ICl) in dry dichloromethane (DCM) (15.0 ml) was added dropwise to a stirred solution of the 4,6-dimethoxy-2-hydroxy-acetophenone (2.55 mmol) in dry dichloromethane (50 ml). The mixture was stirred for 5 h, diluted with dichloromethane (100 ml) and washed with aqueous $Na_2S_2O_3$ (2 × 30 ml), and water (1 × 30 ml). The organic layer was dried ($MgSO_4$) and the solvent was evaporated. The residue was dissolved in petroleum ether-ethyl acetate 1:2 (100 ml), filtered over a short column of silica gel and washed with petroleum ether-ethyl acetate 1:2 (100 ml). The solvent was evaporated, and the residue recrystallized from toluene–petroleum ether to afford product as a white crystalline solid (44%). ^{1}H NMR ($CDCl_3$, 400 MHz) δ: 2.63 (3H, s, CH_3), 3.96 and 3.93 (6H, s, OCH_3), 5.28 (1H, s, CH).

Synthesis of flavones

Step 1. To a solution of appropriate acetophenone (4 mmol) and aldehyde (4 mmol) in C_2H_5OH (25 ml), 20% of aqueous KOH (4 mmol) was added. The reaction mixture was stirred at room temperature till completion of reaction (monitored by TLC). Then the reaction mass was poured into ice water and neutralized with aqueous 10% HCl solution. The precipitate was filtered, washed with excess of water, dried, and recrystallized from methanol to obtain pure chalcones. Step 2. To the solution of appropriate chalcones in dimethyl sulfoxide (10 ml), I_2 (catalytical amounts) was added. The reaction mixture was heated to reflux for 1–2 h, cooled, and poured into water and extracted into EtOAc (3 × 25 ml). The organic layer was washed with brine and dried over $MgSO_4$. The solvent was evaporated to get the product (**F1**–**F5**).

5,7-Dimethoxyflavone (5,7-dimethoxy-2-phenyl-4H-chromen-4-one) (F1)

^{1}H NMR ($CDCl_3$, 400 MHz): δ_H) , 7.87 (2H, d, $J = 7.6$ Hz, Ar H-2′/6′), 7.36-7.44 (3H, m, Ar H-3′,4′,5′), 6.69 (1H, s, H-3), 6.54 (1H, d, $J = 2.0$ Hz, Ar H-8), 6.27 (1H, d, $J = 2.0$ Hz, Ar H-6), 3.92 (1H, s, OCH3), 3.91 (3H, s, OCH3). ^{13}C-NMR (100 MHz, acetone-d_6) δ_C 181.0 (C=O), 170.3 (C-7), 169.1 (C-2), 159.8 (C-5), 147.9 (C-8a), 132.4 (C-1′), 130.9 (C-3′/5′), 129.4 (C-4′), 128.6 (C-2′/6′), 127.9 (C-5a), 110.7 (C-3), 93.8 (C-6), 89.3 (C-8), 55.7 (CH_3), 55.3 (CH_3). ESI-TOF HRMS *m/z*: $[M + H]^+$ 283.0974 (Calc. for $C_{17}H_{15}O_4$, 283.0965) (yellow solid, yield: 59%).

8-Iodo-5,7-dimethoxyflavone (8-iodo-5,7-dimethoxy-2-phenyl-4H-chromen-4-one) (F2)

^{1}H NMR (acetone-d_6, 400 MHz): δ_H 8.18 (2H, m, Ar H-2′/6′), 7.57 (4H, m, Ar-H-3′/4′/5′/6′), 6.75 (1H, s, H-3), 6.68 (1H, s, Ar-H-6), 4.06 (3H, s, OCH_3), 3.96 (3H, s, OCH_3). ^{13}C-NMR (100 MHz, acetone-d_6) δ_C 177.8 (C=O), 168.4 (C-7), 159.6 (C-5), 156.2 (C-8a), 154.3 (C-2), 131.4 (C-4′), 129.2 (C-3′/5′), 126.0 (C-2′/6′), 125.6 (C-1′), 115.8 (C-5a), 108.0 (C-3), 92.9 (C-6), 64.0 (C-8), 56.6 (OCH_3), 55.9 (OCH_3). ESI-TOF HRMS *m/z*: $[M + H]^+$ 408.9930 (Calc. for $C_{17}H_{14}O_4I$, 408.9931) (colorless needle crystal, yield: 85.42%).

6-Methoxyflavone (6-methoxy-2-phenyl-4H-chromen-4-one) (F3)

^{1}H NMR (acetone-d_6, 400 MHz): δ_H 8.07-8.05 (2H, m, Ar H-2′/6′), 7.68 (1H, d, $J = 9.1$ Hz, Ar H-8), 7.57 (2H, m, Ar H-3′/5′), 7.48 (1H, d, $J = 3.2$ Hz, Ar H-4′), 7.37 (1H, d, $J = 9.1$ Hz, Ar H-5), 6.82 (1H, s, H-3), 3.90 (3H, s, OCH_3). ^{13}C-NMR (100 MHz, acetone-d_6) δ_C 177.0 (C=O), 163.3 (C-1), 162.9 (C-6), 157.2 (C-8a), 132.0 (C1′), 131.6 (C-4′), 129.2 (C-3′/5′), 126.3 (C-2′/6′), 124.6

(C5a), 123.2 (C-7), 120.0 (C-8), 106.3 (C-5), 104.9 (C-3), 55.4 (OCH_3). ESI-TOF HRMS *m/z*: $[M+H]^+$ 253.0860 (Calc. for $C_{16}H_{13}O_3$, 253.0859) (orange solid, yield: 58%).

4′-Bromo-6-methoxyflavone (2-(4-bromophenyl)-6-methoxy-4H-chromen-4-one) (F4)

^{1}H NMR (acetone-d_6, 400 MHz): δ_H 8.02 (2H, d, $J=8.7$ Hz, Ar H-3′/5′), 7.76 (2H, d, $J=8.7$ Hz, Ar H-2′/6′), 7.68 (1H, d, $J=8.7$ Hz, Ar H-8), 7.47 (1H, d, $J=3.2$ Hz, Ar H-5), 7.37 (1H, dd, $J=9.1$, 3.2 Hz, Ar H-7), 6.85 (1H, s, H-3), 3.90 (3H, s, OCH_3). ^{13}C-NMR (100 MHz, acetone-d_6,) δ_C 176.9 (C=O), 161.5 (C-1), 157.2 (C-6), 150.8 (C-8a), 132.4 (C-3′/4′), 131.2 (C-1′), 128.1 (C-2′/6′), 125.8 (C-5a), 124.6 (C-4′), 123.3 (C-7), 119.9 (C-5), 106.8 (C-5), 104.8 (C-3), 55.4 (OCH_3). ESI-TOF HRMS *m/z*: $[M+H]^+$ 330.9960 and 332.9937 (Calc. for $C_{16}H_{12}O_3{}^{79}Br$, 330.9970 and $C_{16}H_{12}O_3{}^{81}Br$, 332.9949) (brown solid, yield: 64%).

6,4′-Dimethoxyflavone (6-methoxy-2-(4-methoxyphenyl)-4H-chromen-4-one) (F5)

^{1}H NMR ($CDCl_3$, 400 MHz): δ_H 8.26 (2H, d, $J=9.1$ Hz, Ar H-2′/6′), 7.66 (1H, d, $J=9.1$ Hz, Ar H-8), 7.48 (1H, d, $J=3.2$ Hz, Ar H-5), 7.36 (1H, dd, $J=9.1$, 3.2 Hz, Ar H-6), 7.10 (2H, d, $J=6.9$ Hz, Ar H-3′/5′), 3.91 (3H, s, OCH_3), 3.88 (3H, s, OCH_3). ^{13}C-NMR (100 MHz, acetone-d_6,) δ_C172.4 (C=O), 161.1 (C-2), 156.6 (C-4′), 150.2 (C-6), 145.0 (C-8a), 137.7 (C-1′), 129.7 (C-5a), 129.4 (C-2′/6′), 123.5 (C-7), 121.7 (C-8), 120.0 (C-5), 114.1 (C-3′/5′), 105.1 (C), 103.8 (C-3), 55.5 (OCH_3), 54.8 (OCH_3). ESI-TOF HRMS *m/z*: $[M+H]^+$ 283.0969 (Calc. for $C_{17}H_{15}O_4$, 283.0965) (white solid, yield: 59%).

Molecular docking

Prior to molecular docking, the structures of the compounds were built using Maestro build panels and were optimized and minimized using LigPrep (v3.5.9) in Schrödinger Small Molecule Drug Discovery Suite 2017-1. Molecular docking was performed using Grid-Based Ligand Docking with Energetics (Glide) (v6.8, Schrödinger 2017-1) for human COX and PDE as reported before [20, 21] whereas Genetic Optimization for Ligand Docking (GOLD) 5.2.2 software was used in molecular docking for human 5-LOX [22, 23]. Briefly, the X-ray crystallographic structures of human COX-2 (PDB ID: 3O8Y), 5-LOX (PDB ID: 5F19), PDE4B (PDB ID: 3G45), and PDE4D (PDE ID: 3G4G) were retrieved from Protein Database Bank (PDB, https://www.rcsb.org) [24]. Meanwhile, human COX-1 crystal structure was prepared using homology modeling as described previously [25]. These structures were prepared and optimized using Protein Preparation Wizards. At the end, the crystal structures were minimized using OPLS3 force field [26]. To conduct Glide, the grid generation was generated at the center of the ligand with a grid spacing of 12 Å for COXs and 20 Å for PDEs. The molecular docking for COXs and PDEs was performed using extra-precision (XP) docking mode of Glide software without applying any constraints [27]. For 5-LOX, docking was performed in GOLD by using GoldScore as a scoring function to evaluate the quality of binding pose. Full ligand conformational and partial protein flexibility were considered during the docking [28]. One hundred genetic algorithm (GA) runs were performed for each ligand. All water molecules and hetero atoms were omitted from the protein. The binding region was defined in 10 Å radius around the catalytic iron (Fe2_1_A). The binding interaction patterns of selected compounds in the binding sites of enzymes were visualized using PyMOL (http://www.pymol.org/).

COX peroxidase assay

The inhibitory activity of COX was determined by measuring the formation of oxidized *N*,*N*,*N*′,*N*′-tetramethyl-*p*-phenylenediamine (TMPD) measured spectrophotometrically at 550 nm. The experiment was carried out as previously described with modifications [29]. The COX inhibition reaction was performed by a 10 min incubation at room temperature in the presence of reaction buffer (Tris buffer, 0.1 M, pH 8.0, 150 µl), heme (2.2 mM in DMSO, 10 µl), human recombinant COX-1 or COX-2 enzymes (10 µl), and tested compounds (100 µM in DMSO, 10 µl). The reaction was initiated by adding 20 µL of freshly prepared TMPD and followed by the addition of 20 µL arachidonic acid (diluted with ethanol). The COX activity of compound was compared with celecoxib which is the reference drug. The absorbance was measured using POLARstar Omega multi-mode reader (BMG LABTECH GmbH, Offenburg, Germany) after 5 min of adding arachidonic acid.

5-LOX inhibition assay

The activity of 5-LOX was determined by oxidation of the nonfluorescent substrates, 2′,7′-dichlorodihydrofluorescein diacetate (H_2DCFDA) to the highly fluorescent 2′,7′-dichlorofluorescein (DCF) product during 5-LOX's catalytic reaction [30]. The enzyme assay contained 50 mM Tris (pH 7.5), 2 mM ethylenediaminetetraacetic acid (EDTA), 2 mM $CaCl_2$, 100 µM arachidonic acid and 10 µM H_2DCFDA (pH 7.5). Prior to the addition of studied compounds (dissolved in DMSO), H_2DCFDA and enzyme were preincubated for 5 min. Then the mixture was further preincubated with compounds for another 10 min. The reactions were initiated by the addition of arachidonic acid as substrate. The enzymatic reaction was run for 60 min. Assay plates were read using POLARstar Omega multi-mode plate reader (BMG LABTECH, Offenburg, Germany) under 485 nm excitation and 520 nm emission filters. Fluorescence signals were recorded at 0 and 60 min.

PDE inhibition assay

The PDE activity of compounds was evaluated using PDE-Glo™ Phosphodiesterase Assay kit and the protocol by manufacturer was followed (Promega Corporation, Wisconsin, MI) [31]. Briefly, 1 µl of compounds (final concentration: 100 µM) were preincubated with 1.5 µl of PDE enzyme in 384-well white, flat-bottom plate for 5 min at room temperature. Then 2.5 µl of 2 µM of cAMP was added to initiate the reaction and incubated for 1 h at 37 °C. After incubation

period, termination buffer was added and followed by detection buffer. The mixture was incubated for 20 min at room temperature before the addition of Kinase-Glo®. The mixture was incubated for another 10 min. Luminescence was measured using POLARstar Omega multi-mode plate reader (BMG LABTECH GmbH, Offenburg, Germany).

ADMET prediction

ADMET properties of flavones were predicted using ADMETlab [32] and QikProp [33] in Schrodinger Small Drug Discovery Suite 2017-1. On the other hand, ProTox-II (http://tox.charite.de/protox_II) [34], ACD/i-Lab 2.0 (https://ilab.acdlabs.com/iLab2) [35], and Pred-hERG 4.1 (http://labmol.com.br/predherg) [36], a free web-based service were used to analyze the toxicity profiles of flavones.

Cytotoxicity assay

Cytotoxicity of compounds against RAW 264.7 cells was determined using MTT assay [37]. 100 µl of compounds (serial dilution in media, 0–100 µM) was treated with 10,000 cells/well for 24 h at 37 °C in 5% CO_2 under 70% humidity. Then, 10 µl of MTT dye (5 mg/ml in PBS) was added to each well. The plate was incubated again for 4 h. The supernatant was then aspirated out and was replaced with 100 µl of lysis solution (DMSO). After 30 min of incubation, the absorbance was read at 595 nm and the percentage of cell viability was calculated. Data were analyzed using sigmoidal dose-response (variable slope) equation or four-parameter logistic curve (4PL) in GraphPad Prism®, version 7.03, for Windows® (GraphPad Software, La Jolla, CA).

Results and discussion

Chemistry

All the compounds were synthesized according to the steps outlined in Figure 1. The chalcone derivatives (**C1**, **C3**, **C4**, and **C5**) were prepared *via* Claisen–Schmidt condensation reaction of readily accessible acetophenones and benzaldehydes in the presence of 20% sodium hydroxide in ethanol at room temperature for 24 h. While synthesis of chalcone derivatives **C2** begun through iodonization of 4,6-dimethoxy-2-hydroxy-acetophenone with iodine monochloride in dry acetone at room temperature for 5 h. Targeting flavones (**F1**–**F5**) were synthesized by refluxing corresponding chalcones in DMSO in the presence of iodine as catalyst. All the synthesized flavones were confirmed on the basis of their spectroscopic evidence. In the ^{1}H NMR spectra of **F1**–**F5**, olefinic proton attached to the C-3 appeared as a singlet in the range of δ_H 5.69–6.90, while singlet signals from methoxy protons appeared at δ_H 3.87–4.03. Besides that, aromatic protons attached to the ring A and C appeared as a singlet, doublet and multiplate in the range of δ_H 5.28–8.13.

Docking scores

The activity of synthesized flavones toward COXs, 5-LOX, and PDEs were analyzed *via* molecular docking study (Table 1). Based on docking study of COX, the structure of all the synthesized flavones able to dock with COX-1 and COX-2 binding cavities resulting docking scores less than −7 kcal/mol but only **F2** exhibited selectivity toward COX-2. The reference drug, celecoxib, however, is the only able to dock inside the COX-2 binding cavity. In the case of docking to 5-LOX, the flavones had GOLD fitness score in a range of 13.45 and 54.62 which were slightly less than the reference drug, zileuton (GoldScore = 57.00). **F2** in 5-LOX showed the lowest fitness score while **F5** possessed the highest fitness score. The bulky structure of **F2** may affect the accessibility of **F2** to the substrate channel in the closed conformation of 5-LOX. Hence, **F2** was unable to bind perfectly at the active sites of LOX. Small compounds otherwise had good fitness score. The present study also found that **F1**–**F3** exhibited comparable docking scores in PDEs with the reference drug, rolipram but only **F1** and **F3** were more selective to PDE4B as compared to rolipram. The other flavones showed low binding affinity to both PDEs with docking scores more than −5 kcal/mol.

Inhibitory activity of flavone derivatives

To validate the result of docking, the activities of compounds were evaluated through inhibition assay. For COXs and PDEs, only compounds with the SI more than 1 were tested for the inhibitory activity while all docked compounds to 5-LOX were proceeded with inhibition assay (Table 2). From the results, **F2** was more selective to COX-2 as compared to COX-1 which was similar to the result of docking. However, the selectivity of **F2** toward COX-2 was lower than celecoxib by two-fold but the activity of inhibition against COX-2 was comparable with celecoxib.

In PDEs, **F1** and **F3** were chosen for determining PDE activity. Although there was a slight difference in SI of docking scores between **F1** and **F3**, **F3** showed four times more selective to PDE4B than PDE4D in inhibition assay while **F1** showed is selective to PDE4D with SI less than 1. Moreover, SI of PDE4B of **F3** was higher than that of rolipram. This indicated that the position of methoxy group in the benzene ring of chromone played an important role in the selectivity of flavones where *para*- position was more favorable in biological activity than *meta*-position.

For 5-LOX, **F5** has the highest inhibition against 5-LOX but less than zileuton. The inhibition scores were lower for **F2**, followed by **F4** and **F3** while no activity of 5-LOX was observed in **F1**. The result suggested that *para*- position of methoxy group (**F3**) was more favorable than *meta*-position (**F1**) for inhibition of 5-LOX. The substitution of halogen group, iodine at 8-position in **F2** substantially decreased the activity of 5-LOX as compared to **F1**. The paramount role of halogen in improving drug efficacy was reported earlier [38,39]. The addition of functional group at *para*- position in

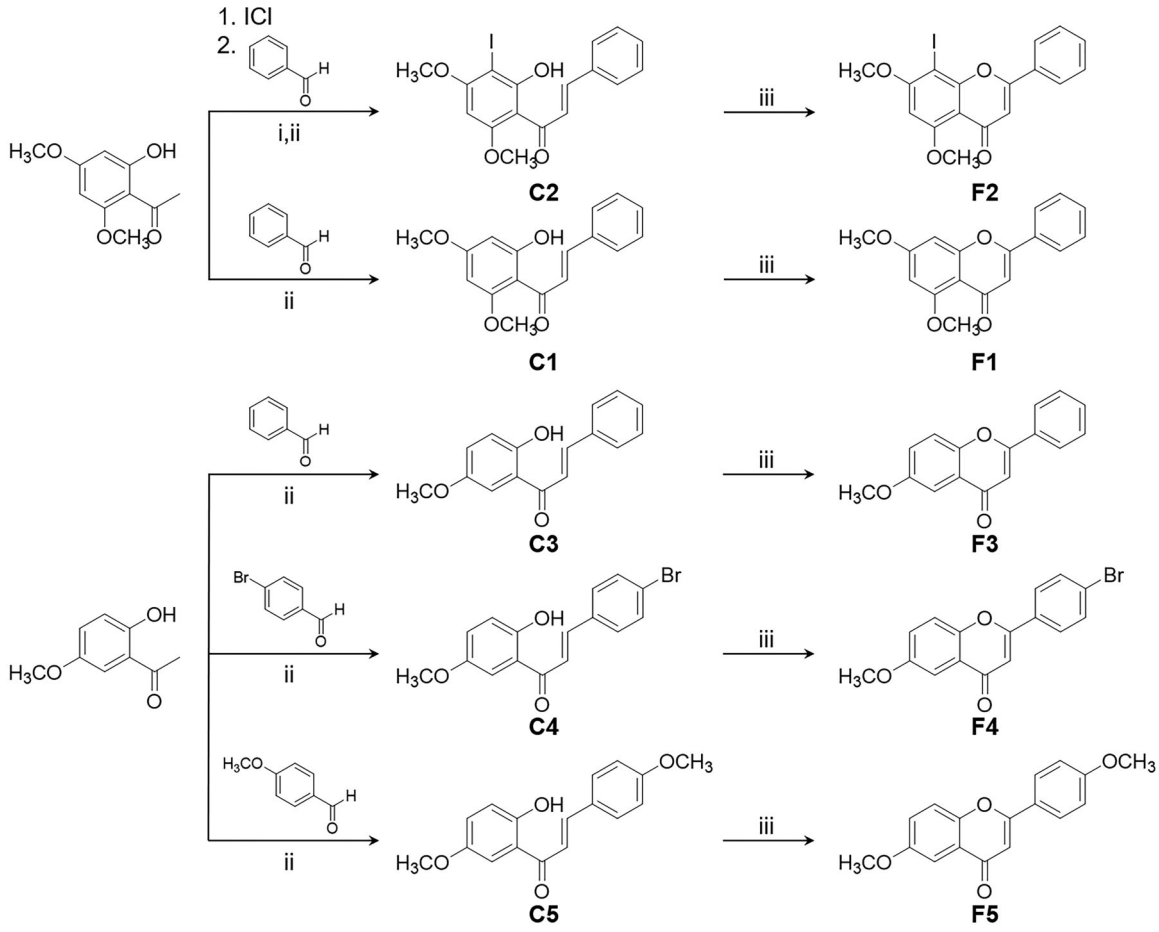

Figure 1. Schematic diagram of flavone synthesis. Reaction condition: (i) ICl, dry DCM, room temperature, 5 h; (ii) KOH 20%, ethanol, room temperature, 24 h; (iii) I2, DMSO, reflux 2 h.

Table 1. Binding score of compounds toward respective targets.

Compounds	Docking score (kcal/mol)				GOLD fitness score
	COX-1	COX-2	PDE4B	PDE4D	5-LOX
Celecoxib	ND	−11.869	–	–	–
Rolipram	–	–	−9.368	−9.576	–
Zileuton	–	–	–	–	57.00
F1	−8.019	−7.987	−10.530	−9.191	49.99
F2	−8.351	−9.281	−8.814	−9.229	13.45
F3	−9.316	−8.641	−9.932	−8.782	53.12
F4	−9.460	−8.792	−1.367	−4.675	52.97
F5	−8.883	−8.512	−3.992	−4.568	54.62

ND: not dock; – : not determined.

phenyl ring further enhanced the inhibitory activity of 5-LOX where methoxy was more favorable (**F5**) than bromine (**F4**).

Analysis of binding interactions

The active compounds were further evaluated for their binding modes in the target sites. The investigation of the binding interaction of celecoxib in COX-2 active site revealed that sulfonamide phenyl group of celecoxib occupied the side pocket of COX-2 binding site and formed hydrogen bond with H90 (2.4 Å), L352 (2.2 Å), and F518 (2.7 Å) (Figure 2(a)). The interaction in the side pocket of COX-2 confers selectivity of celecoxib toward COX-2 compared to compound **F2**. Besides, imidazole group of celecoxib formed cation-π interaction with R120 at the entrance of binding site. Meanwhile, phenyl group of celecoxib was stabilized by hydrophobic interactions *via* strong van der Waals interaction in hydrophobic region of binding site which composed of M522, F381, L384, Y385, W387, and A527. In contrast, the selectivity of **F2** was contributed by the addition of iodine group involved in the van der Waals forces and increased the binding affinity to COX-2 (Table 3) [40]. **F2** only occupied a part of COX-2 active site which was mostly at the hydrophobic region and entrance of binding site. These explained the difference of selectivity for COX-2 in both compounds. The orientation of **F2** was firmly fixed by the formation of π–π interaction between phenyl group and W387 and cation-π interaction between ring A of **F2** and R120. Further, **F2** was stabilized by hydrophobic interactions of active site amino acid V349, Y355, L359, F381, L384, Y385, W387, F518, M522, V523, A527, and L531 (Figure 2(c)). In addition, binding pose of **F2** in COX-1 remained unchanged but the absence of side pocket in COX-1 made **F2** to move deeper to hydrophobic region of COX-1. This resulted in the formation of additional π-π interaction with Y385 along with W387. The phenyl of **F2** was then stabilized by hydrophobic interaction of F381, L384, Y385, W387, F518, and M522 whereas the chromone part of F2 was stabilized by hydrophobic interaction of V116, V349, L352, Y355, L359, I523, and L531 (Figure 2(b)).

Table 2. Percentage of inhibition of enzymes at single concentration (100 μM) of compounds.

	Percentage of Inhibition (%)						
Compounds	COX-1	COX-2	SI of COX-2	PDE4B	PDE4D	SI of PDE4B	5-LOX[a]
Celecoxib	13.02 ± 2.84	98.20 ± 2.55	7.54	–	–	–	–
Rolipram	–	–	–	51.87 ± 0.38	66.51 ± 2.49	0.78	–
Zileuton	–	–	–	–	–	–	90.81 ± 0.19
F1	–	–	–	50.05 ± 4.46	74.31 ± 3.22	0.67	NA
F2	25.41 ± 5.71	98.96 ± 1.47	3.90	–	–	–	20.96 ± 11.20
F3	–	–	–	39.70 ± 5.19	8.50 ± 3.96	4.67	7.30 ± 6.11
F4	–	–	–	–	–	–	16.99 ± 9.72
F5	–	–	–	–	–	–	33.65 ± 4.74

Values were presented in mean ± SD. a: concentration of compounds at 10 μM; SI: selectivity index; NA: not active; – : not determined.

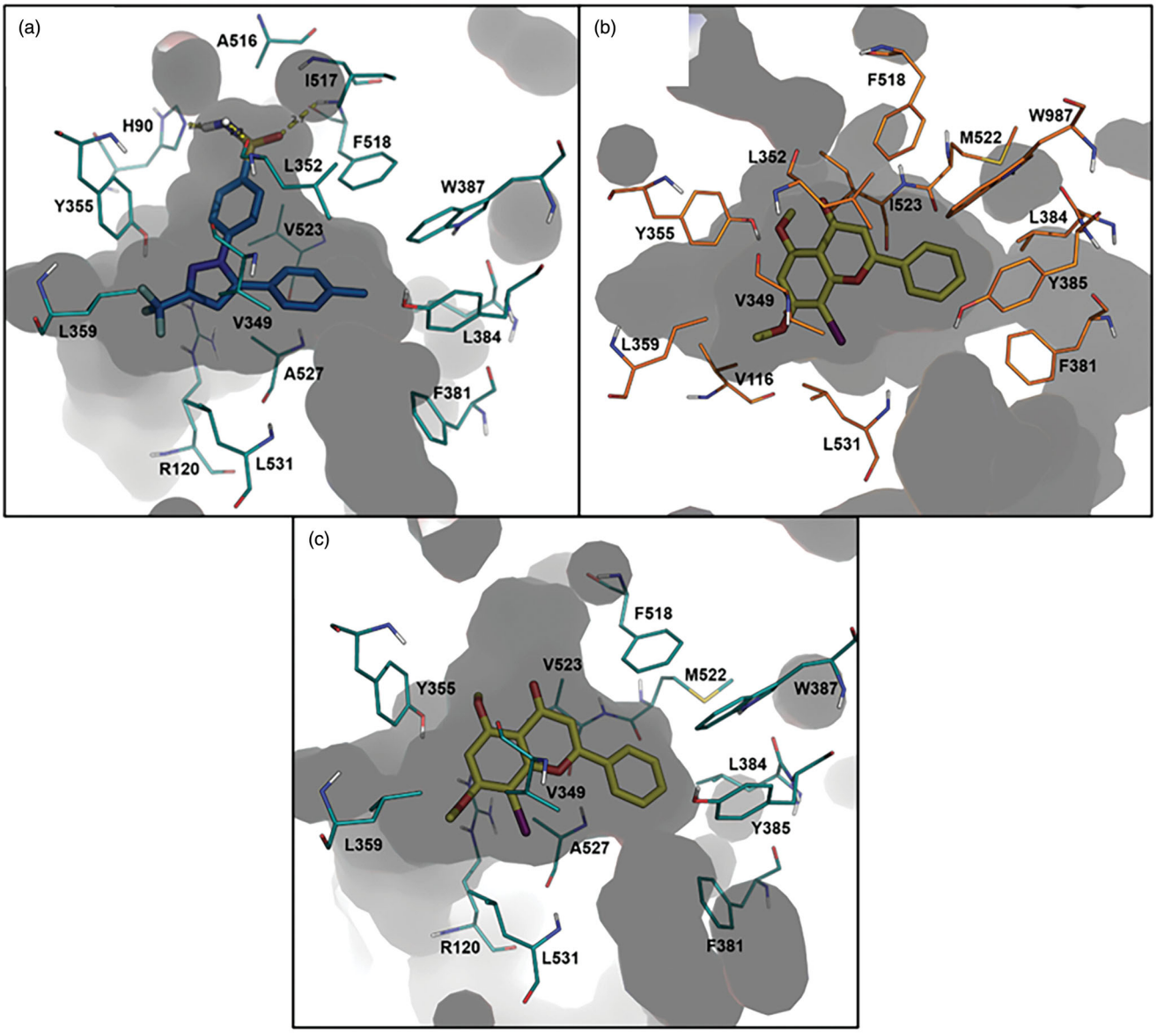

Figure 2. Binding mode of celecoxib in COX-2 (a) active site and F2 in COX-1 (b) and COX-2 (c) active site.

Analysis of binding interaction of rolipram in PDE showed that rolipram bind to active sites of PDE4B (Figure 3(a)) and PDE4D (Figure 3(b)) in similar orientation and interacted with the same residues. Thus, rolipram had lack of selectivity toward PDE4B. Rolipram formed two hydrogen bonds with key interacting residues, glutamine (Q615 in PDE4B and Q535 in PDE4D) (1.8–2.4 Å) which involved in substrate binding and established numerous interactions with residues of active sites. The phenylmethoxy ring of rolipram sat in a hydrophobic pocket of PDE4, interacting with Y274, F279, I582, F585, and F618 in PDE4B and F196, I502, F506, and F538 in PDE4D. The pyrrolidone group of rolipram anchored in the direction of highly conserved metal binding pocket and formed hydrophobic interactions with F279, Y405, L565,

Table 3. Binding energy of the celecoxib and **F2** in COX binding sites.

	COX-1/(kcal·mol^{-1})				COX-2/(kcal·mol^{-1})			
Comp.	LE	evdw	En	emodel	LE	evdw	En	emodel
Celecoxib	–	–	–	–	−0.456	−48.821	−47.910	−75.511
F2	−0.380	−10.528	−10.528	23.848	−0.411	−38.743	−38.698	−39.453

LE: Glide ligand efficiency; evdw: Glide Van der Waals energy; En: Glide energy; emodel: Glide model energy.

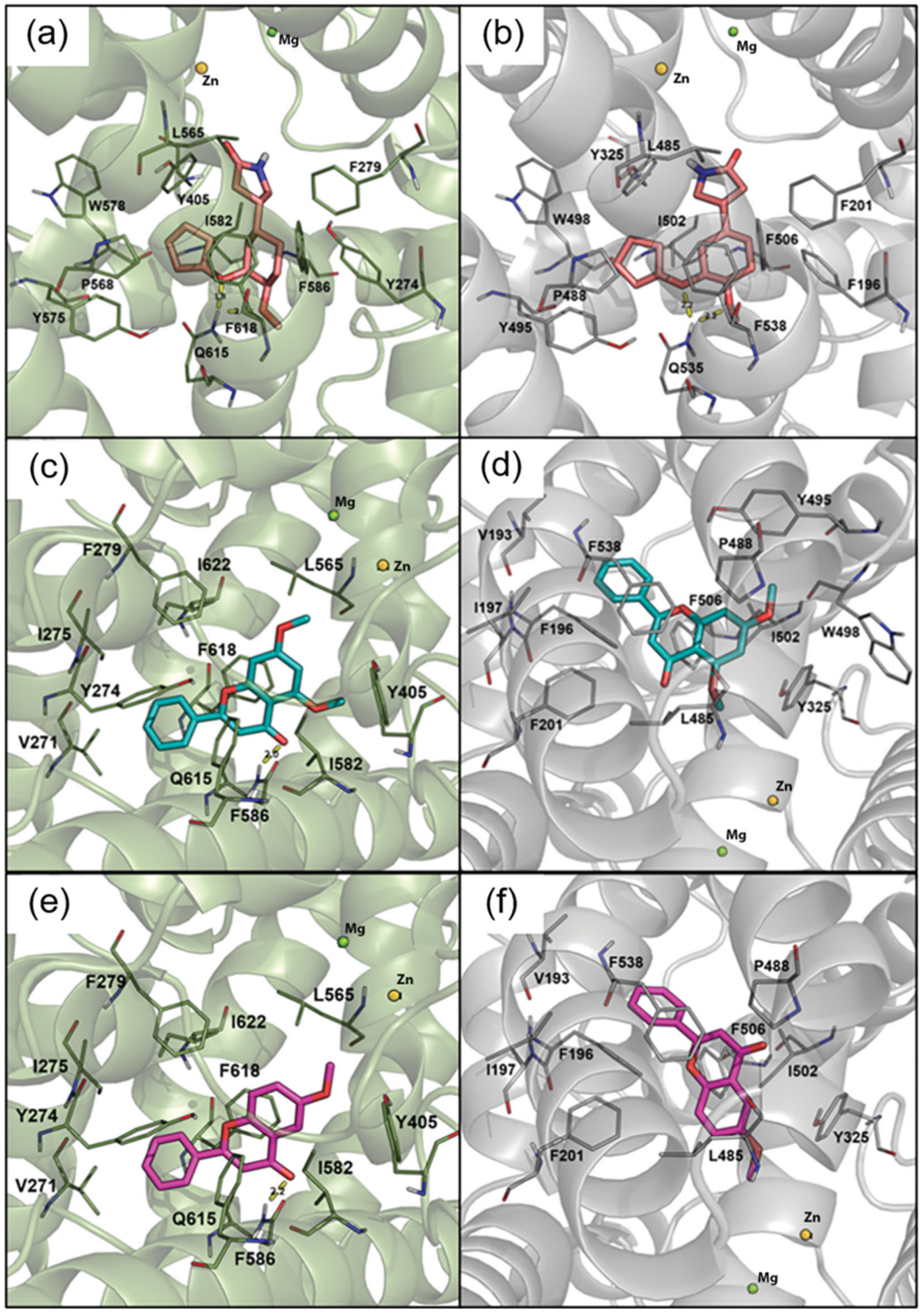

Figure 3. Binding mode of rolipram in PDE4B (a) and PDE4D (b) active site, F1 in PDE4B (c) and PDE4D (d) active site and F3 in PDE4B (e) and PDE4D (f) active site. Zinc and magnesium were depicted in sphere, respectively.

and I582 in PDE4B and F201 and L485 in PDE4D. On the other hand, the cyclopentyloxy group of rolipram interacted with Y405, P568, Y575, W578, I582, and F618 in PDE4B and Y325, P488, Y495, W498, and I502 in PDE4D *via* van der Waals interactions. The study also found that hydrogen bonding plays important role in binding interaction of rolipram.

The binding patterns of **F1** and **F3** in PDE4B (Figure 3(c,e), respectively) were the same, while there were differences of binding modes in PDE4D. This is due to the orientation of I275 in PDE4B and I197 in PDE4D. The orientation of propane side chain of I275 which buried into the pocket creates additional space in side pocket of PDE4B. As a result, **F1** bound deeper into the side pocket and allow the bulky **F1** to fit in whereas smaller side pocket in PDE4D changed the binding position of **F1**. The comprehensive exploration of binding mode of flavones revealed that the heterocyclic structure of chromone in **F1** and **F3** had occupied Q pocket of PDE4B while the ketone group formed strong hydrogen bond (2.0–2.2 Å) with side chain of Q615. This possibly prevented the interaction between substrate and enzyme, thus leading to inhibition of PDE4B. Moreover, both flavones were flanked between I582 and F618 and made π–π interaction with Y274 and F618. Their position was further stabilized by hydrophobic interaction of conserved residues including Y274, Y405, L565, I582, F586, and F618.

In PDE4D, the phenyl ring of **F1** and **F3** were projected to be at the entrance of active site. However, the orientation of chromone ring of **F1** and **F3** were distinctive. The chromone part of **F1** laid on Q pocket of PDE4D (Figure 3(d)) while the chromone part of **F3** occupied the metal binding pocket of PDE4D (Figure 3(f)). The position of **F1** resulted in the establishment of π–π stacking with Y325 and F538 in opposite direction which gave more stable binding position in **F1** than **F3**. Moreover, hydrophobic interactions (Lipophilic EvdW + PhobEn) with surrounding residues which include V193, F196, I197, F201, Y325, L485, P488, Y495, W498, I502, F506, and F538 increased stabilization of **F1** in the binding pocket of PDE4D (Figure 4). **F3** only formed single π–π stacking between ring B and F538. **F3** also stabilized itself through hydrophobic interactions of V193, F196, I197, F201, Y325, L485, P488, F506, and F538. Therefore, **F3** became less selective to PDE4D as compared to **F1**.

The prediction of binding interaction in 5-LOX suggested that hydrogen bond had significant contribution in binding interaction of zileuton (Figure 5(a)). Hydroxyl group of zileuton formed strong hydrogen bond with Q363 (1.9 Å) while two hydrogen bonds were formed between ketone group of zileuton and N425 (2.0 Å) and H600 (2.6 Å). The position of zileuton in the binding pocket was further stabilized by hydrophobic interaction of F177, Y181, L368, L414, F421, and L607 at benzothiophene group and F359, A603, and V604 at the hydroxyurea group. In contrast, the interaction of **F5** in 5-LOX was contributed by Van der Waals forces as indicated in Table 4 and possessed different binding position as compared to zileuton. Strong hydrophobic interactions were formed between **F5** and hydrophobic residues of 5-LOX involving F177, L368, F359, A410, L414, F421, V604, A603, and L607 (Figure 5(e)).

On the other hand, the steric effect of halogen group in **F2** caused the orientation of **F2** to flip oppositely from **F5** in the active site of 5-LOX. Iodine at ring A then made a contact with N425 (3.3 Å) to form halogen bond and chromone at ring B formed hydrogen bond with Q363 (2.5 Å). Hydrophobic interactions stabilized the position of **F2** that involved F177, A410, L368, L414, and I415 at the phenyl ring of **F2** and F359, F421, A603, V604 and L607 at chromone group of **F2** (Figure 5(b)). The position of **F4** in binding pocket of 5-LOX is also the same with **F2** which was supported by hydrophobic interaction of F177, Y181, L414, L420, F421, A424, W599, A603, V604, and L607. The interaction was strengthened by π–π interaction (edge-to-face) between ring A and phenyl ring of F421 (Figure 5(d)). **F3** possessed similar orientation as **F5** but shifted toward polar region of 5-LOX. This resulted in the formation of hydrogen bond between chromone part of **F3** and Q363 (2.6 Å). It was stabilized by L368, L414, F421, and L607 at chromone part of **F3** and Y181, L420, A424, W599, A603, and V604 at phenyl part of **F3** (Figure 5(c)).

ADMET properties

Failing the criteria of ADMET is the major reason for drug rejection in development of drug. Therefore, this study used two software to predict ADMET properties of compounds. QikProp is a commercial software that calculate prominent ADMET descriptors of compounds. Another software, ADMETlab is a free web interface software which comprehensively performs systematic evaluation of ADMET of compounds based on 288,967 ADMET data entries collected. In addition to two software, ProTox-II was used to predict the average lethal dose (LD_{50}) in rodents and toxicity of compounds according to Tox21 criteria. This study also used Pred-hERG to specifically assess hERG inhibition of compounds while ACD/i-Lab predicts LD_{50} of compounds in different route of administration and health effects of compounds.

Data revealed that all compounds successfully conceded the Lipinski's rule of five which is a druglikeness assessment (Table 5) [41]. It was also observed that all compounds had satisfactory bioavailability as indicated in Tables S1 and S2. With respect to metabolism of compounds, all compounds were predicted to be metabolized by CYP1A2, CYP2C9, CYP2C19, and CYP2D6. Moreover, all compounds had high probability to act as inhibitor of CYP3A4. This affected the bioavailability, the toxicity, and the effectiveness of compounds [42]. The half-lives and clearance rates of the compounds were low but within the acceptable range. Though, the toxicities vary across the compounds.

Human ether-a-go-go related gene (hERG K^+) potassium channel involves in modulating electrical activity of the heart that coordinates heart's beating. Hence, the blockage of hERG K^+ can cause fatal arrhythmia which is the main concern in developing new therapeutic drugs. The compounds were non-blocker of hERG K^+ channel according to the

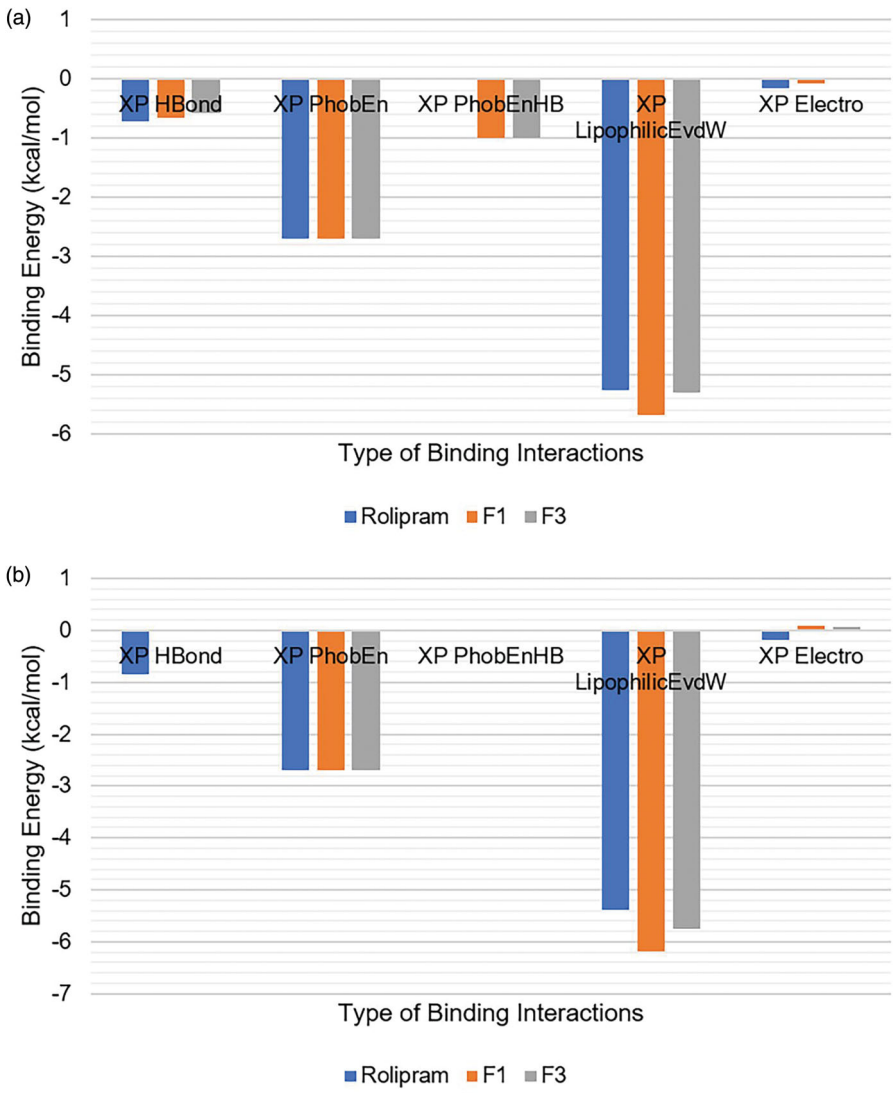

Figure 4. Binding energy of rolipram and selected flavones in PDE4B (a) and PDE4D (b). XP Hbond: ChemScore H-bond pair term; XP PhobEn: hydrophobic enclosure reward; XP LipophilicEvdW: lipophilic term derived from hydrophobic grid potential at the hydrophobic ligand atoms; XP Electro: electrostatic rewards which includes Coulomb and metal terms.

results shown by two softwares (ADMETlab and Pred-hERG) (Tables S1 and S2). The LD_{50} values for the acute toxicity analyses using ADMETlab showed that **F2** and **F4** had moderate toxicity while **F1**, **F3**, and **F5** had low toxicity (Table S1). Contrarily, ProTox-II had classified **F2**–**F5** to class V ($2000\,mg/kg < LD50 \leq 5000\,mg/kg$) and **F1** to class IV ($300\,mg/kg < LD50 \leq 2000\,mg/kg$) based on oral toxicity in rats with high similarity and prediction accuracy (Table S3).

LD_{50} plots for each compound calculated using ACD/i-Lab were also compared (Figure 6(a)). The degree of safety route of administration from the safest in the compounds was oral > subcutaneous > intraperitoneal > intravenous. **F1** had the highest LD_{50} whereas others had similar LD_{50}. From toxicological end point evaluation of compounds, the prediction showed that all compounds did not cause immunotoxicity. Ames test which determines the mutagenicity of compounds was negative in all compounds despite had moderate probability to cause carcinogenicity. The compounds also did not showed toxicity in liver but may cause severe drug-induced liver injury (DILI), the frequent cause of drug withdrawal [43]. This was in line with the prediction of health effects of compounds where **F2** had the highest probability to affect liver besides cardiovascular (CV) and gastrointestinal tract (GIT) (Figure 6(b)). The compounds may also affect blood and kidney while lung is the least affected organ.

Cytotoxicity

The cytotoxicity data revealed that **F3**–**F5** were not toxic to the cells at 100 μM (Table 6). Otherwise, **F1** was moderate toxic and **F2** had the lowest IC_{50} among all compounds. The result proved that the position of methoxy group influenced the inhibitory properties of the compounds and affected their cytotoxicity. The flavones with *para*- position of methoxy exhibited less toxicity in comparison with *meta*-

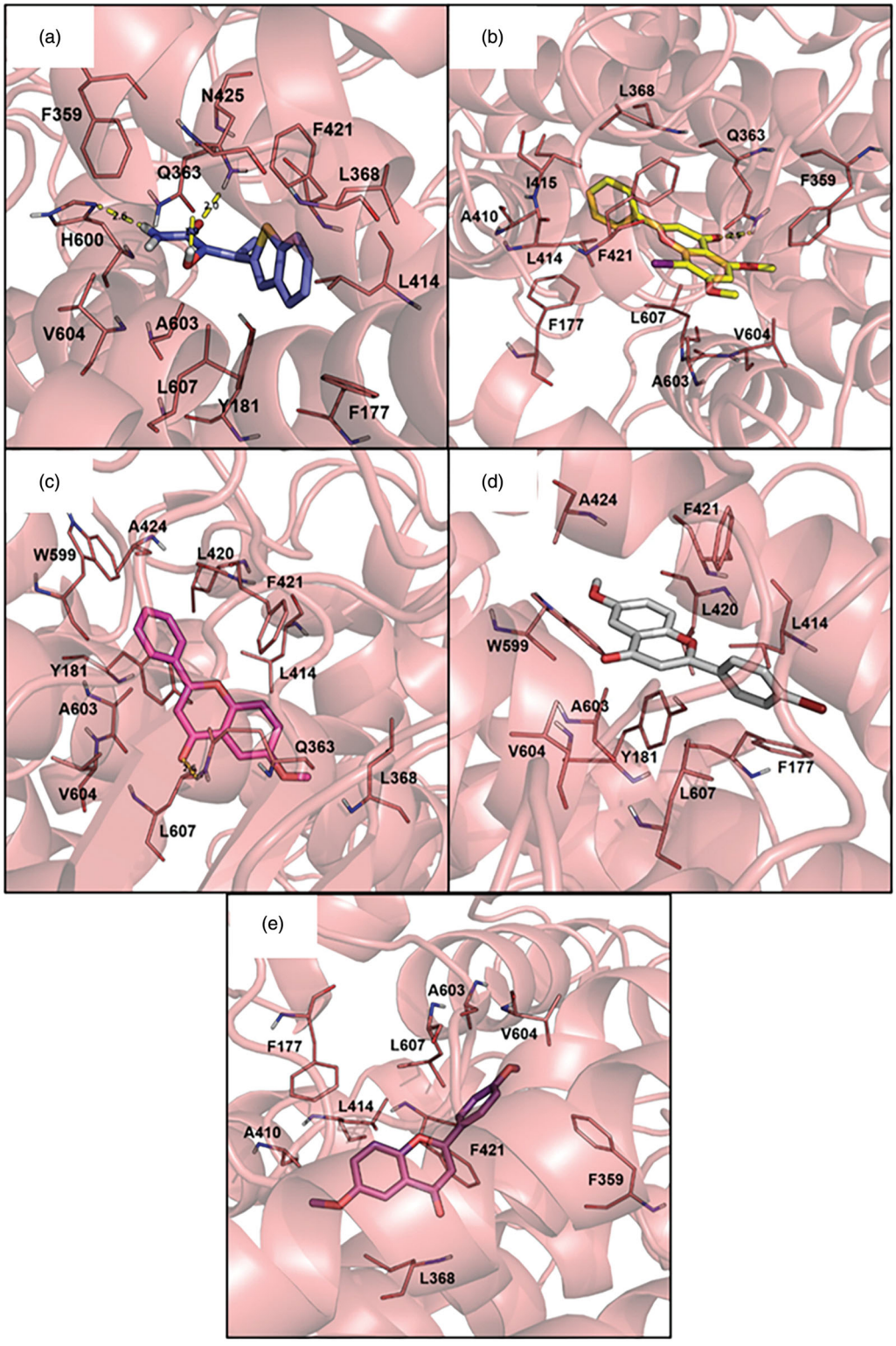

Figure 5. Binding mode of zileuton (a), F2 (b), F3 (c), F4 (d), and F5 (e) in 5-LOX active site.

position of methoxy. The incorporation of halogen group further increases the toxicity of flavones (**F2**). The risk of toxic potential of halogenated lead compounds had been discussed before and became a major concern in designing drug [40,44].

Conclusions

The studied compounds (**F1**–**F5**) demonstrated different degree of selectivity toward different inflammatory targets. Amid these compounds, **F2**, **F3**, and **F5** had potential as initial scaffold for further development of selective inhibition

Table 4. Binding energy of the zileuton and flavones in 5-LOX binding site.

Compound	Fitness score	S_{hb_ext}	S_{vdw_ext}	S_{hb_int}	S_{int}
Zileuton	57.00	2	40.53	0	−0.74
F2	53.12	0.08	36.74	0	−0.23
F3	13.45	1.16	12.44	0	−5.09
F4	52.97	0.27	40.53	0	−3.03
F5	54.62	0	42.19	0	−3.39

$Shb_{\_ext}$: contribution of protein–ligand hydrogen bond to GoldScore value; S_{vdw_ext}: contribution of van der Waals to GoldScore value; $Shb_{\_int}$: contribution of intracellular hydrogen bonds to GoldScore value; S_{int}: contribution of intramolecular strain in the ligand to GoldScore value.

Table 5. Drug-likeness properties of flavones derivatives using QikProp.

Compounds	Molecular weight	HB Acceptor	HB Donor	Log *P*
F1	282.295	4	0	3.477
F2	408.191	4	0	4.082
F3	252.269	3	0	3.469
F4	331.165	3	0	4.231
F5	282.295	4	0	3.477

for COX-2, 5-LOX, and PDE4B, respectively. The potency of the compounds linked with the position of methoxy group which need to be retained. However, the presence of iodine may cause toxic effect as showed in **F2**. Thus, the replacement of iodine with less reactive halogen group needs to be considered to decrease the toxicity of the compounds. These key features need to be emphasized in future optimization of these promising scaffold.

Table 6. Cytotoxicity of flavone derivatives.

Compounds	IC_{50} (μM)
F1	78.61 ± 1.329
F2	16.02 ± 1.165
F3	>100
F4	>100
F5	>100

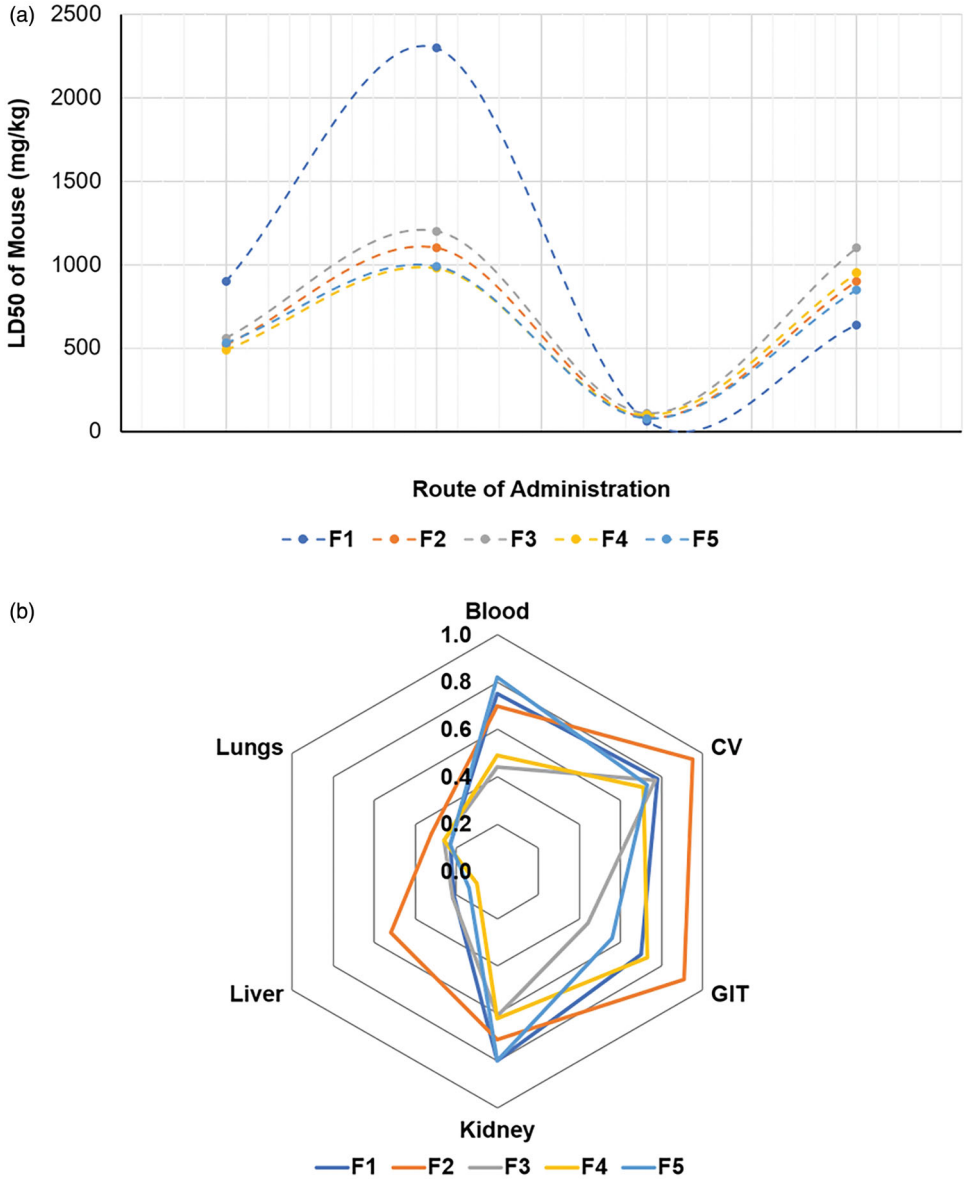

Figure 6. LD50 of mouse (intraperitoneal, oral, intravenous, subcutaneous) graph plot for **F1–F5** (a) and probability of health effects of **F1–F5** on organs (b).

Acknowledgments

The authors would also like to thank Integrative Pharmacogenomics Institute (iPROMISE), UiTM (Grant no. 241910/2015/MZS/7) for providing financial assistance and facilities to carry out related research work. The in vitro synthesis steps, computational modelled data and efficacy of the compounds as anti-inflammatory agents had been submitted for patent application (Application no. PI 2018704123).

Disclosure statement

No potential conflict of interest was declared by the authors.

Funding

This work was supported by Ministry of Higher Education (MOHE), Malaysia under Transdisciplinary Research Grant Scheme [Grant no. 600-RMI/TRGS 5/3 (1/2014)].

ORCID

Muhd Hanis Md Idris http://orcid.org/0000-0001-8246-6493
Siti Norhidayah Mohd Amin http://orcid.org/0000-0002-3382-0019
Zainul Amiruddin Zakaria http://orcid.org/0000-0001-5525-7821
Zurina Shaameri http://orcid.org/0000-0002-0314-8532
Ahmad Sazali Hamzah http://orcid.org/0000-0002-6826-1659
Manikandan Selvaraj http://orcid.org/0000-0001-8604-8598
Mohd Zaki Salleh http://orcid.org/0000-0001-9882-0661

References

[1] Chen L, Deng H, Cui H, et al. Inflammatory responses and inflammation-associated diseases in organs. Oncotarget. 2018;9(6):7204–7218.
[2] Martel-Pelletier J, Lajeunesse D, Reboul P, et al. Therapeutic role of dual inhibitors of 5-LOX and COX, selective and non-selective non-steroidal anti-inflammatory drugs. Ann Rheum Dis. 2003;62(6):501–509.
[3] Kaminska B. MAPK signalling pathways as molecular targets for anti-inflammatory therapy-from molecular mechanisms to therapeutic benefits. Biochim Biophys Acta. 2005;1754(1–2):253–262.
[4] Zheng XY, Chen JC, Xie QM, et al. Anti-inflammatory effect of ciclamilast in an allergic model involving the expression of PDE4B. Mol Med Rep. 2019;19:1728–1738.
[5] Brune K, Patrignani P. New insights into the use of currently available non-steroidal anti-inflammatory drugs. J Pain Res. 2015;8:105–118.
[6] Khan YS, Gutiérrez-de-Terán H, Åqvist J. Molecular mechanisms in the selectivity of nonsteroidal anti-inflammatory drugs. Biochemistry. 2018;57(7):1236–1248.
[7] Li H, Zuo J, Tang W. Phosphodiesterase-4 inhibitors for the treatment of inflammatory diseases. Front Pharmacol. 2018;9:1048.
[8] Bruno F, Spaziano G, Liparulo A, et al. Recent advances in the search for novel 5-lipoxygenase inhibitors for the treatment of asthma. Eur J Med Chem. 2018;153:65–72.
[9] Tungmunnithum D, Thongboonyou A, Pholboon A, et al. Flavonoids and other phenolic compounds from medicinal plants for pharmaceutical and medical aspects: an overview. Medicines. 2018;5(3):16–93.
[10] Verma AK, Pratap R. The biological potential of flavones. Nat Prod Rep. 2010;27(11):1571–1593.
[11] Pérez-Cano FJ, Castell M. Flavonoids, inflammation and immune system. Nutrients. 2016;8(10):659.
[12] Azam S, Ansari P, Rashid M, et al. *In vitro* anti-oxidant and *in vivo* anti-inflammatory activity determination of the methanolic leaves extract of *Millettia pachycarpa*. Biomed Res Ther. 2015;2:366–373.
[13] Farzaei MH, Singh AK, Kumar R, et al. Targeting inflammation by flavonoids: novel therapeutic strategy for metabolic disorders. IJMS. 2019;20(19):4957.
[14] Barik R, Sarkar R, Biswas P, et al. 5,7-Dihydroxy-2-(3-hydroxy-4, 5-dimethoxy-phenyl)-chromen-4-one-a flavone from *Bruguiera gymnorrhiza* displaying anti-inflammatory properties. Indian J Pharmacol. 2016;48(3):304–311.
[15] Dzoyem JP, Nkuete AHL, Ngameni B, et al. Anti-inflammatory and anticholinesterase activity of six flavonoids isolated from Polygonum and Dorstenia species. Arch Pharm Res. 2017;40(10):1129–1134.
[16] Chen L, Teng H, Xie Z, et al. Modifications of dietary flavonoids towards improved bioactivity: an update on structure-activity relationship. Crit Rev Food Sci Nutr. 2018;58(4):513–527.
[17] Sharma A, Sharma P, Tuli H, et al. Phytochemical and pharmacological properties of flavonols. In: eLS. Chichester: John Wiley & Sons, Ltd.; 2018. p. 1–12.
[18] Yusof MIM, Salleh MZ, Kek TL, et al. Activity-guided isolation of bioactive constituents with antinociceptive activity from *Muntingia calabura* L. leaves using the formalin test. Evidence-based complement. Altern. Med. 2013;2013:1–27.
[19] Serafini M, Peluso I, Raguzzini A. Flavonoids as anti-inflammatory agents. Proc Nutr Soc. 2010;69(3):273–278.
[20] Gaddipati RS, Raikundalia GK, Mathai ML. Dual and selective lipid inhibitors of cyclooxygenases and lipoxygenase: a molecular docking study. Med Chem Res. 2014;23:1–14.
[21] Tripuraneni NS, Azam MA. Pharmacophore modeling, 3D-QSAR and docking study of 2-phenylpyrimidine analogues as selective PDE4B inhibitors. J Theor Biol. 2016;394:117–126.
[22] Cole JC, Nissink JWM, Taylor R. Protein-ligand docking and virtual screening with GOLD. In: Alvarez J, Shoichet B, editors. Virtual screening in drug discovery. 1st ed. Florida: CRC Press; 2005. p. 388–424.
[23] Jones G, Willett P, Glen RC, et al. Development and validation of a genetic algorithm for flexible docking. J Mol Biol. 1997;267(3):727–748.
[24] Berman HM, Westbrook J, Feng Z, et al. The protein data bank. Nucleic Acids Res. 2000;28(1):235–242.
[25] Md Idris MH, Mohd Amin SN, Selvaraj M, et al. High-throughput structure-based drug design of chalcones scaffolds as dual inhibitor of cyclooxygenase-2 and microsomal prostaglandin E synthase-1. J Pharm Sci Emerg Drugs. 2018;6:1–14.
[26] Shivakumar D, Williams J, Wu Y, et al. Prediction of absolute solvation free energies using molecular dynamics free energy perturbation and the OPLS force field. J Chem Theory Comput. 2010;6(5):1509–1519.
[27] Friesner RA, Banks JL, Murphy RB, et al. Glide: a new approach for rapid, accurate docking and scoring. 1. Method and assessment of docking accuracy. J Med Chem. 2004;47(7):1739–1749.
[28] Kutil Z, Kvasnicova M, Temml V, et al. Effect of dietary stilbenes on 5-lipoxygenase and cyclooxygenases activities *in vitro*. Int J Food Prop. 2015;18(7):1471–1477.
[29] Wisastra R, Kok PA, Eleftheriadis N, et al. Discovery of a novel activator of 5-lipoxygenase from an anacardic acid derived compound collection. Bioorg Med Chem. 2013;21(24):7763–7778.
[30] Pufahl RA, Kasten TP, Hills R, et al. Development of a fluorescence-based enzyme assay of human 5-lipoxygenase. Anal Biochem. 2007;364(2):204–212.
[31] Promega. 2016. PDE-GloTM Phosphodiesterase Assay. https://www.promega.com/-/media/files/resources/protocols/technical-bulletins/101/pde-glo-phosphodiesterase-assay-protocol.pdf.
[32] Dong J, Wang NN, Yao ZJ, et al. ADMETlab: a platform for systematic ADMET evaluation based on a comprehensively collected ADMET database. J Cheminform. 2018;10(1):29.
[33] QikProp. Schrödinger Release 2017-1: QikProp. New York (NY): Schrödinger, LLC; 2017.

[34] Banerjee P, Eckert AO, Schrey AK, et al. ProTox-II: a webserver for the prediction of toxicity of chemicals. Nucleic Acids Res. 2018; 46(W1):W257–W263.
[35] Masunov A. ACD/I-Lab 4.5: an internet service review. J Chem Inf Comput Sci. 2001;41(4):1093–1095.
[36] Braga RC, Alves VM, Silva MFB, et al. Pred-hERG: a novel web-accessible computational tool for predicting cardiac toxicity. Mol Inform. 2015;34(10):698–701.
[37] Meerloo J, Van Kaspers GJL, Cloos J. Cell sensitivity assays: the MTT assay. In: Cree IA, editor. Cancer Cell Cult. 2nd ed. London: Humana Press; 2011. p. 237–245.
[38] Makkar F, Chakraborty K. First report of dual cyclooxygenase-2 and 5-lipoxygenase inhibitory halogen derivatives from the thallus of intertidal seaweed *Kappaphycus alvarezii*. Med Chem Res. 2018;27(10):2331–2340.
[39] Xu Z, Yang Z, Liu Y, et al. Halogen bond: its role beyond drug-target binding affinity for drug discovery and development. J Chem Inf Model. 2014;54(1):69–78.
[40] Hernandes MZ, Cavalcanti SM, Moreira DR, et al. Halogen atoms in the modern medicinal chemistry: hints for the drug design. Curr Drug Targets. 2010;11:1–12.
[41] Lipinski CA. Lead- and drug-like compounds: the rule-of-five revolution. Drug Discov Today Technol. 2004;1(4):337–341.
[42] Zhang Z, Tang W. Drug metabolism in drug discovery and development. Acta Pharm Sin B. 2018;8(5):721–732.
[43] Xu Y, Dai Z, Chen F, et al. Deep learning for drug-induced liver injury. J Chem Inf Model. 2015;55(10):2085–2093.
[44] Kortagere S, Ekins S, Welsh WJ. Halogenated ligands and their interactions with amino acids: implications for structure-activity and structure-toxicity relationships. J Mol Graph Model. 2008;27: 70–177.